Solid State Sciences 92 (2019) 24–30

Contents lists available at ScienceDirect

Solid State Sciences

journal homepage: www.elsevier.com/locate/ssscie

Evaluation of cryo-treatment in the luminescent properties of PVDF/Eu_2O_3 composite obtained by using buriti oil as additive

Airton Germano Bispo-Jr[a,b], Ana Maria Pires[a,b], Sergio Antonio Marques Lima[a,b], Celso Xavier Cardoso[a,*]

[a] São Paulo State University (Unesp), School of Technology and Sciences, Presidente Prudente, SP, 19060-900, Brazil
[b] São Paulo State University (Unesp), Institute of Biosciences, Humanities and Exact Sciences, São José do Rio Preto, SP, 15054-000, Brazil

ARTICLE INFO

Keywords:
Polymer
Eu(III)
Natural oil
PVDF composite

ABSTRACT

Polymeric matrices containing luminescent particles find many applications like temperature sensor platforms. However, it is important to understand the impact of the particle immobilization on the polymer structural and optical properties in order to optimize its performance. Therefore, in this study, a new luminescent polymeric composite was fabricated by combining poly (vinylidene fluoride) (PVDF), buriti oil (BO) and Eu_2O_3 particles, evaluating the membrane luminescent properties before and after a cryo-treatment with liquid N_2 in order to enhance the Eu(III) emission. Also, the influence of Eu_2O_3 particles and BO in the polymer structural, thermal, morphological and optical properties was evaluated. The composite membranes with bandgap lying between 5.60 and 5.90 eV were obtained as γ-PVDF phase after being dried at 100 °C, with spheroidal particles connected by necks. The PVDF membranes are very stable till temperatures as high as 370 °C, and the Eu_2O_3 particle addition increases the membrane thermal stability while the BO decreases the PVDF stability. The cryo-treatment with N_2 increases the PVDF crystallinity, leading to the PVDF particles agglomeration. The PVDF/BO/Eu_2O_3 membrane exhibited the characteristic red emission from Eu(III) along with an unexpected BO emission. Finally, after the cryo-treatment, the Eu^{3+} emission increases while the BO emission vanishes, and due to this temperature sensitivity, the system shows potential to be applied in temperature sensor platforms.

1. Introduction

Over the past few years, photoluminescent sensors based on rare earth in polymer matrices have received great attention because of their potential application in various devices. [1,2,3] In such composites, the luminescent properties coming from rare earth oxides (RE oxides) play the important role of providing a specific functionality or the improvement of the optical properties with respect to the polymers [4]. This synergism, between the polymer and RE oxide properties, is a promising alternative for new composite materials synthesis which could be applied in several devices as gas sensors [5], chemosensors [6], light emitting diodes [7], full-color displays [8], etc. Besides that, the use of additives as buriti oil in the membrane synthesis is very common because the additive molecules penetrate the polymeric matrix and act as lubricants between the polymeric chains, improving the flexibility and processability of polymers [9].

The Polyvinylidenefluoride (PVDF, $C_2H_2F_2$) is a semi-crystalline polymer extensively studied in a wide range of applications [10], being able to act as a polymer matrix due to its easy processing, high mechanical strength, excellent mechanical property, thermal stability, high chemical resistance and high hydrophobicity compared to other commercialized polymeric materials [11]. This polymer is also used as a matrix for nano- or micron-sized particles. [12,13,14] Several methods are employed in the fabrication of PVDF membranes and these include the use of inorganic particles as a filler or as an additive, sintering, phase inversion and track etching. [15,16]

The buriti oil (from *Mauritia flexuosa* L.), BO, is an oil commonly found in the Amazon region with red-orange color and compound by fatty acids (~78% oleic acid), tocopherols (~800 mg kg^{-1}) and carotenes (~70% beta-carotene). [17,18] The fatty acids present in the buriti oil have long chains (more than 10 carbon atoms in their structure) [19]. The BO can be used as a plasticizer in polymeric materials [20] as reported for poly (methyl methacrylate) (PMMA) and polystyrene (PS) [21], or in starch films [22]. Also, we recently reported the synthesis and the luminescent properties of the PVDF/$Ba_2SiO4:Eu^{3+}$ red light emitting membrane using BO as plasticizer [23].

* Corresponding author. São Paulo State University (Unesp), School of Technology and Sciences, R. Roberto Simonsen, 305, 19060-900, Presidente Prudente, SP, Brazil.
E-mail address: xavier.cardoso@unesp.br (C.X. Cardoso).

https://doi.org/10.1016/j.solidstatesciences.2019.04.003
Received 21 June 2018; Received in revised form 24 September 2018; Accepted 6 April 2019
Available online 09 April 2019
1293-2558/

Europium ions, Eu(III), have been largely studied because of their long emission lifetime, high efficiency and narrow emission bands in the visible region, [24,25]characteristics that appoint europium ions to be used in a wide range of applications as full-color displays, tunable lasers or light-emitting diodes. [26,27] The main emissions in the visible region are originated from the Eu(III) $^5D_0$ excited state to the ground $^7F_{0\text{-}6}$ levels. Eu_2O_3 is a rare earth sesquioxide used to synthesize phosphors, as control rods in nuclear reactors and transistor devices [28] and it has two common structures, cubic with space group *Ia*-3 and monoclinic with space group C2/*m*. [29] Some studies have reported the use of Eu(III) compounds in a polymeric matrix. For example, Martins et al. used Gd_2O_3:Eu^{3+} in PVDF composite for scintillator application [30]. J. Garcia-Torres et al. studied the influence of different polymeric matrix on the spectroscopic properties of Eu(III) complexes [31]. Although Eu_2O_3 itself has low emission, its luminescent properties still can be used for applications that use the luminescent signal as a sensor.

There are many methods to improve the polymer performance regarding its structural and optical features, such as control and design of bulk properties, filler/fiber reinforcement, interpenetrating network (IPN) structure development, surface modifications or cryo-treatment [32]. In the present report, the method chosen for the intensification of polymer membrane luminescence was the cryogenic treatment in liquid N_2, since it is a simple, fast and low-cost technique for modifying the polymer mechanical, structural and optical properties. For the best of our knowledge, there is no paper reported in the literature about the improvement of the Eu(III)-luminescence in a polymeric matrix by cryo-treatment with N_2. Therefore, considering the synergism between the mechanic properties of the polymer and the Eu_2O_3 luminescence, we report in this study the fabrication of red light emitting PVDF composite membranes containing Eu_2O_3 particles obtained by casting method using buriti oil as a plasticizer. We also investigated the cryo-treatment with liquid N_2 to enhance the luminescent properties of the composite.

2. Experimental section

The PVDF/BO/Eu_2O_3 membrane was prepared applying the "casting" method by using dimethylformamide (10 mL) as the solvent and PVDF (2.0000 g, ATOCHEM), buriti oil (250 μL, mundo dos oleos, $\rho_{23\,°C}$ = 0.92 g/cm^3) and Eu_2O_3 (0.0250 g, SIGMA-ALDRICH, 99.99%). The suspension was stirred at 80 °C for 2 h for the PVDF and the oil dissolution and after that, it was transferred to a Petri dish with a diameter of 9 cm and dried at 100 °C for 6 h. PVDF containing BO membrane and pure PVDF membrane were synthesized as control and they were prepared by the same method used for the PVDF/BO/Eu_2O_3 membrane. Then, the PVDF/BO/Eu_2O_3 composite membrane was immersed in liquid N_2 at - 160 °C for 1 min.

The PVDF membranes were characterized by X-Ray Diffraction (XRD) using a Shimadzu model 600 diffractometer; by scanning electron microscopy (SEM) using a Carls Zeiss model EVO LS15 scanning electron microscope with a detector of secondary electron (SE) in a high vacuum and at constant temperature; by thermogravimetric (TGA) and differential scanning calorimetry (DSC) analysis using a Universal V45A TA Instruments, static air atmosphere, and a heating ramp of 10 °C min^{-1}, from 30 °C up to 600 °C; by diffuse reflectance using a Varian model Cary 500 Scan using as standard solid MgO; and by photoluminescence spectroscopy using a PerkinElmer model LS55 spectrometer equipped with continuous Xe lamp (9.9 W) excitation. Lifetime measurements were carried out by using a pulsed Xe arc lamp (6 mJ/pulse) coupled to a Kratos GM-252 monochromator and a Spex 1934 C phosphorimeter.

3. Results

The semi-crystalline structure of PVDF membranes was characterized by X-ray diffraction, Fig. 1. The Eu_2O_3 powder itself exhibits diffraction peaks attributed to the JCPDS-32-380 card with cubic structure and space group *Ia-3* (206). Already for the PVDF membranes, the XRD profile exhibit two halos at 2θ = 20.3° and 18.7° which dominate the XRD pattern for the membranes (except for the PVDF/BO/Eu_2O_3 membrane) that are assigned to PVDF γ-phase formation [33]. The diffraction peaks profile indicates low crystallinity of the membranes and the PVDF semi-crystalline nature. Furthermore, a peak at 2θ = 18.4° with low intensity is attributed to the PVDF α-phase, showing a low percentage of α-phase in the membranes [34]. Gregorio et al. showed that a portion of the α-phase always remains in the PVDF composition because the transformation occurring in the ringed spherulites at high temperature seems to be never complete [35]. In the α-PVDF phase, the chains adopt the *trans*-cis-type conformational structure (TCTC), which is thermodynamically more stable because it allows the greatest possible distance from the fluorine atoms. In the γ-phase chains, to each three *trans*-conformations, a cis conformation occurs ($T_3C\ T_3C$-) [36]. The existence of γ phase in the PVDF membranes depends on the mobility of conformers in the solution which mainly is affected by the thermal energy because this is not the most thermodynamically stable PVDF phase [37]. The membranes were prepared at 100 °C and the thermal energy is high enough to rotate CF_2 groups in the monomer, resulting in a cooperative motion of the neighboring CF_2 groups through the large-scale *trans*-gauch conformational change, which is enough to obtain γ phase.

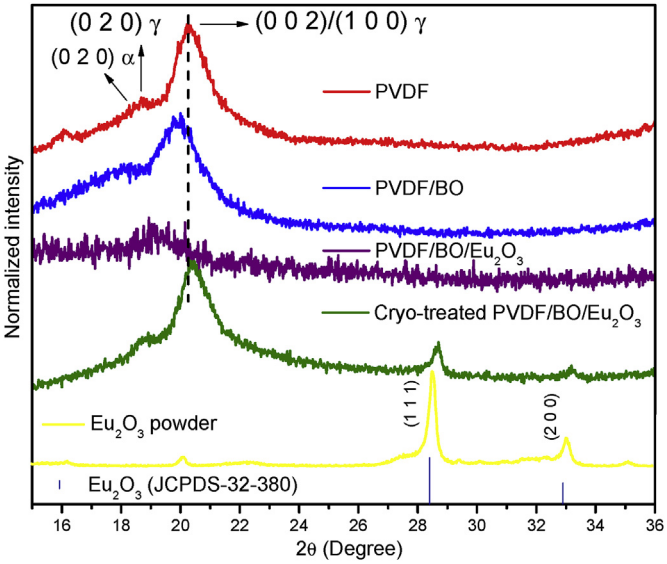

Fig. 1. X-ray diffractograms of PVDF membranes.

The PVDF/BO/Eu_2O_3 membrane does not exhibit the γ-PVDF profile, but an amorphous structure, indicating that PVDF crystallization is inhibited by Eu_2O_3 particles. Song et al. obtained similar results for La_2O_3-doped PVDF membranes [38]. Yet, after the cryogenic treatment, the γ-PVDF profile is observed again, showing that the process is organizing the PVDF chains, increasing the crystallinity of PVDF polymer. The addition of BO and Eu_2O_3 and also the cryo-treatment causes a displacement in the position of γ-PVDF plans in relation to the pure PVDF membrane. These modifications can be related to variations in the PVDF chain size and organization, in the degree of crystallinity or changes in the strengths that maintains the chains interaction. Before the cryogenic treatment in the PVDF/BO/Eu_2O_3 membrane, the XRD profile does not show diffraction peaks attributed to the Eu_2O_3 phase, but they are observed after the cryogenic treatment because, before the cryogenic treatment, the PVDF halo in the XRD pattern covers the Eu_2O_3 peaks.

The morphology of the membranes was checked by SEM measurements, Fig. 2, in order to evaluate whether the addition of BO, Eu_2O_3

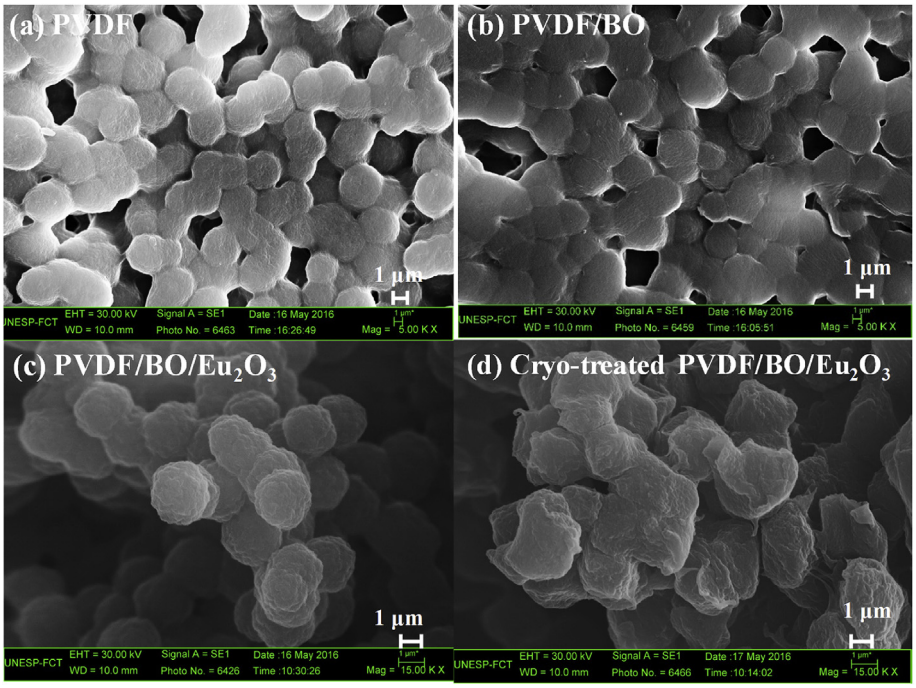

Fig. 2. Scanning electron microscopy (SEM) images of the membranes for (a) pure PVDF, (b) PVDF/BO, (c) PVDF/BO/Eu_2O_3, and (d) PVDF/BO/Eu_2O_3 treated with liquid N_2.

and the cryogenic treatment would have some influence on the shape of the membranes. SEM images for the Eu_2O_3 powder, Figure S1, show that the particles are submicron-sized with irregular shape. Fig. 2 reveals microstructures formed by fused spheroidal particles in the PVDF, PVDF/BO and PVDF/BO/Eu_2O_3 membrane surface with diameter around 4 µm for the PVDF and PVDF/BO membranes that decreases to approximately 2 µm when Eu_2O_3 was added in the membrane. Similar microstructure was obtained by Shi et al. for PVDF membranes containing TiO_2 particles [39]. The addition of BO and Eu_2O_3 does not modify the microspheroidal structure. On the other hand, after the cryo-treatment of the membrane, the particle became more irregular in shape and more agglomerated. Besides that, the surface texture of the untreated polymer appeared to be quite smooth compared to the rough topography of the cryo-treated surface. Indumathi et al. reported a similar behavior for PTFE (Polytetrafluoroethylene) and (Polyethylenimine) polymers [40] attributing the enhanced roughness of the surface to the contraction caused by the cryogenic treatment and then the uneven expansion when the membrane is brought back to the ambient temperature. Therefore, in the PVDF/BO/Eu_2O_3 cryo-treated membrane, the residual stresses caused by the contraction force might have been responsible for the change within the particles too. This process is also known as fracture and it occurs because usually, the polymer fracture resistance decreases when temperature decreases from room temperature to the liquid N_2 one. The fracture is a process well-know in the literature and it is reported for other kind of polymers as LaRC PETI-5, LaRC 5050, and LCR [41].

Thermogravimetric analyses for the PVDF membranes are displayed in Fig. 3. The PVDF membranes are very stable till temperatures as high as 370 °C. The PVDF decomposition occurs in two steps, the first between 400 and 500 °C and the second between 500 and 600 °C in accordance with the literature [42]. The high stability of the membranes could be correlated with the high electronegativity of the fluorine atoms belonging to the polymer chain and their high C—F bond dissociation energy. Above that temperature, the PVDF begins to degrade forming hydrogen fluoride, the monomer and small amounts of $C_4H_3F_3$, as reported in the literature [43]. The thermal decomposition of Buriti oil also takes place in two steps, the first near to 260 °C is due to the

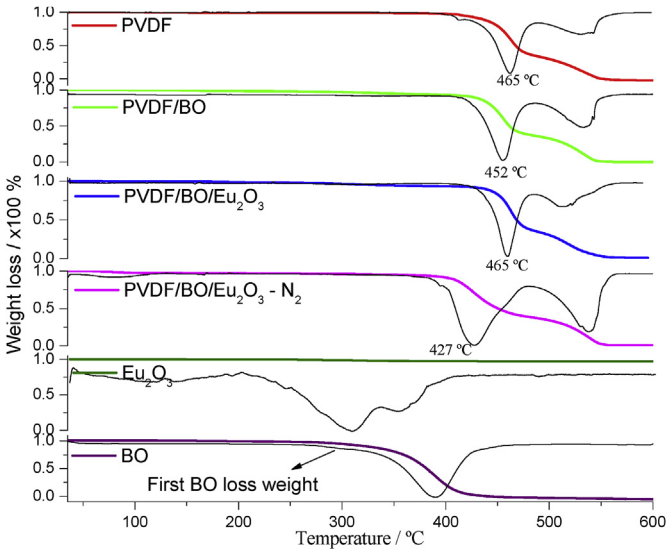

Fig. 3. Thermograms (TG) and Differential thermogravimetry (DTG, black lines) for the synthesized PVDF membranes compared to the Eu_2O_3 powder and BO liquid precursors.

release of volatile components and the second around to 425 °C indicates the complete breakdown of fatty acids [21]. For the membranes containing BO, it is observed a weight loss around 300 °C achieving a plateau between 300 and 450 °C due to the BO decomposition. Already the Eu_2O_3 powders are very stable till temperatures as high as 600 °C, with a small weight loss at 300 °C probably due to some carbonate that is formed on the particle surface.

The membrane containing BO have smaller degradation temperature than the pure PVDF, as represented in the DTG curves, Fig. 3, suggesting that the BO leads to a PVDF thermal stability decreases. However, the Eu_2O_3 addition increases the PVDF temperature degradation when compared to the PVDF/BO membrane and consequently, the PVDF stability. Similar profile was also observed by Al-

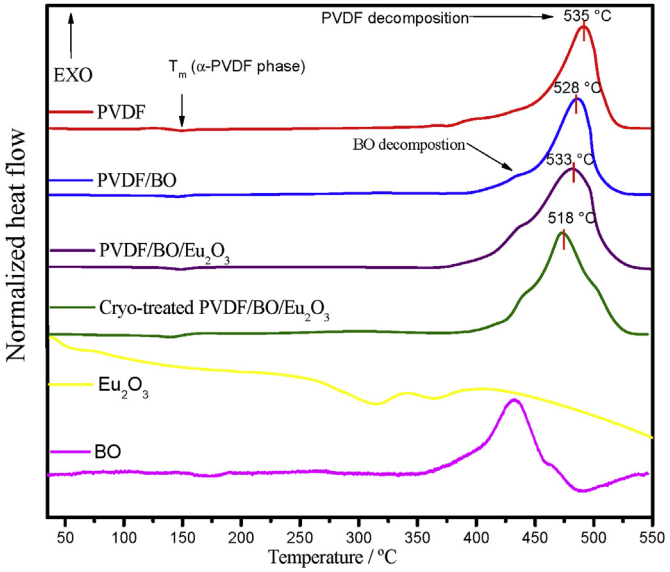

Fig. 4. DSC scans of PVDF membranes compared to the BO liquid precursor.

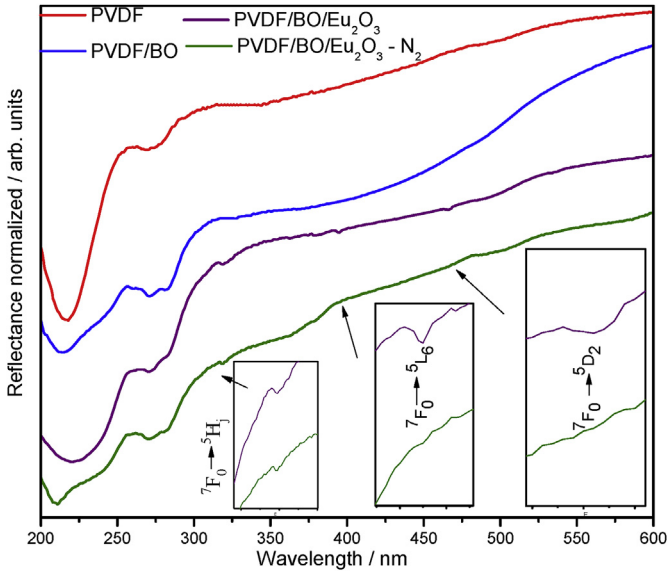

Fig. 5. UV–Vis diffuse reflectance spectra of PVDF membranes.

Hazmi et al. for Cu_2O particles in PVDF membranes [44]. The thermal stability improvement due to the Eu_2O_3 particles incorporation in the PVDF may be related to the packing of the crystalline γ-phase around Eu_2O_3 particles [45]. In this way, the proximity between the PVDF chains and the rare earth oxide particle surface can generate superficial interactions, providing an increase in the thermal stability behavior of PVDF chains because they are more strongly bonded in the composite than if they were alone in the membrane. For the cryo-treated membrane, a weight loss near to 100 °C is observed and probably is due to the membrane water absorption during the cryo-treatment with liquid N_2. After the cryo-treatment, the membrane stability decreases, probably due to the cracks and tensions created during the contraction-expansion cycle.

The DSC analysis gives further insight into the thermal behavior of the membranes as illustrated in Fig. 4. For the Eu_2O_3 powder, two thermal events at about 313 °C and 362 °C can be noticed in the DSC scan and they are in accordance with the TG measurements previously discussed. The DSC scans exhibit two peaks for the PVDF membranes, one nearly 530 °C (exothermic) assigned to the PVDF decomposition as shown in the TG curves and other at 170 °C (endothermic), due to the melting of α-PVDF [46], indicating that exist PVDF in the α-form in accordance with the XRD data. The influence of BO, Eu_2O_3 and cryogenic treatment on the thermal stability of PVDF was evaluated through the comparison of the thermal decomposition temperature of the membranes. Again, after the addition of BO, the PVDF degradation temperature slightly decreases, as observed in the TG measurements. The PVDF decomposition temperature also decreases after the cryo-treatment, confirming that the polymer thermal stability decreases.

Diffuse reflectance spectra were acquired in the UV–Vis region, Fig. 5, for PVDF membranes. A broadband centered at ~216 nm is observed in the DR spectra and it is attributed to PVDF absorption indicating its semi-crystalline nature. [47,48,49] Furthermore, the membranes containing Eu_2O_3 display absorption lines at 320, 395 and 467 nm attributed to Eu(III) absorption from the $^7F_0$ state to ^5H_j, $^5L_6$ and $^5D_2$ excited states, respectively. These lines have more intense absorption before the cryo-treatment.

By diffuse reflectance technique, it is possible to calculate the optical bandgap value of the membranes. Through a graphic of $(\alpha h\nu)^n$ versus the energy of the incident photon (h), Figure S2, where *n* has a value equal to 2 for direct transition and 0.5 for indirect transition, the curve extrapolation to zero provides the optical bandgap energy [50]. The value of α is the ratio of the absorption and scattering coefficients according to the approximation of Kubelka-Munk [51], Equation (1), where R is the reflectance observed for the different incident energies. A previous study showed that the samples had better profile considering direct transitions (See Figure S3). The bandgap for direct transitions lies between 5.70 and 5.90 eV and it varies with the presence of BO, Eu_2O_3 and the cryogenic treatment, as shown in Table 1. This behavior may be associated with the structural and compositional changes verified by XRD data occurring after the addition of the BO, Eu_2O_3 and the cryo-treatment. This variation in the optical energy values can be related to the formation of defects in the polymer structure (band rupture, free radical, etc.) which can be associated to the semi-crystalline or the amorphous structure of PVDF and the relation between the PVDF-phases. When these defects are generated, associated energy levels can lie between the valence band and conduction band, and as consequence, lead to a modification in the band gap values.

$$\alpha = \frac{K}{S} = \frac{(1-R)^2}{4R} \quad (1)$$

Before the PL analysis for PVDF membranes, it was performed the PL measurements of buriti oil dissolved in ethanol, Fig. 6, where it is observed five emission bands around 442, 458, 500 and 515 nm and three excitation bands around 316, 346 and 366 nm. The excitation and emission of BO are dependent on the excitation or emission wavelength. This occurs because the different components of BO exhibit different emission or excitation wavelengths, being very difficult to assign the emission to each BO components. Albuquerque et al. showed that it is possible to attribute the BO emission to some compounds of BO, but the origin of the oil can influence the composition of the extract [20].

The PVDF membranes excitation and emission spectra at room temperature are shown in Fig. S4. In the excitation spectra for the pure PVDF and PVDF/BO membranes, Figure S4 (a), it is observed week broadbands centered at 316 and 368 nm in the ultraviolet spectral

Table 1
Band gap values calculated from Kubelka-Munk approximation considering direct transitions for all synthesized membranes.

Membrane	Bandgap/eV
PVDF	5.70
PVDF/BO	5.80
PVDF/BO/Eu_2O_3	5.60
Cryo-treated PVDF/BO/Eu_2O_3	5.91

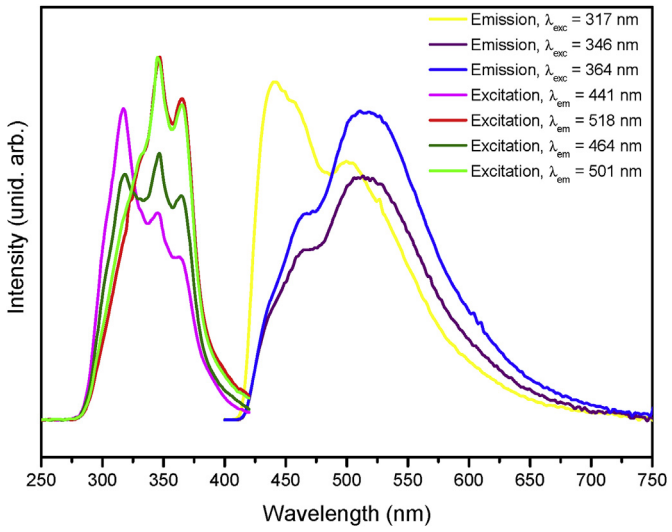

Fig. 6. Excitation and emission spectra of buriti oil dissolved in ethanol (10% V/V).

range attributed to PVDF excitation. Srivastava et al. reported the UV–Vis absorption spectra of PVDF, wherein it is shown that PVDF has five characteristic bands at 315 nm, 325 nm, 360 nm, 425 nm and 600 nm which were correlated with the electronic transition occurring in C—F bonds [47]. In this way, the PVDF radiation absorption in the UV or visible spectral region involves the electrons promotion in σ and n-orbitals from the ground state to higher energy states. In this case, these states can be generated as a result of C—F simple bonds [52].

Considering the PVDF/BO/Eu_2O_3 and the cryo-treated PVDF/BO/Eu_2O_3 membrane, a broad charge transfer band (CT) around 267 nm dominates the excitation spectra, Fig. 7(a). This characteristic band is associated with Eu^{3+}-O^{2-} interactions. Narrow peaks with relatively low intensity can also be observed and they are associated with the *f-f* Eu(III) transitions that are forbidden by the Laporte's rule. In this region, it is also observed a broadband from 350 nm to 500 nm assigned to the BO excitation that overlaps the *f-f* transitions. However, the intensity of this band decreases after de cryo-treatment.

In the PVDF and PVDF/BO membranes, no significant emission is detected in the emission spectra under 267 nm excitation, just a week band near to 350 nm, Figure S4(b). But for the PVDF/BO/Eu_2O_3 membranes, the corresponding emission spectra under 267 nm excitation exhibit the set of $^5D_0 \rightarrow {}^7F_{0,1,2,3,4}$ transitions in the red region assigned to the Eu(III) in low-symmetry sites [53], which profile is very similar to the Eu_2O_3 powder, Fig. 7 (b) (A photograph of the membrane under white light and UV radiation exposition is shown in Figure S5). Besides, it is possible to see two broad bands at 410 and 435 nm which are attributed to BO emissions since PVDF has no emission in this region, and the band are very similar to those previously shown for the pure BO in Fig. 6. However, this BO emission is not expected in this case since the BO has no absorption under 267 nm excitation (See Fig. 6). This BO anomalous emission can be explained by an energy transfer mechanism involving Eu_2O_3 particles and the BO molecules. When the excitation light with 267 nm excites the Eu^{3+}-O^{2-} charge transfer band, the energy from this state usually decay non-radiatively to the $^5D_0$ emitting state of the europium (III) ion. However, if BO and Eu_2O_3 are close enough in the membrane, it is possible that Eu(III) ions transfer energy to excited states of BO molecules, resulting in BO emission. Considering the PVDF/BO/Eu_2O_3 membrane, the $^5D_0 \rightarrow {}^7F_2$ transition of Eu(III) and BO emission have similar intensities, but after the cryo-treatment, the $^5D_0 \rightarrow {}^7F_2$ emission increases and the BO emission decreases. This behavior could be explained by the fact that before the cryo-treatment, the bonds in the BO components must change its conformation due to the compression previously showed by SEM measurements, modifying the energy levels. In this case, due to these structural modifications, the BO emission is not observed because the new energy levels are probably not favorable to the energy transfer and, as consequence, the $^5D_0$ population increases, favoring the Eu(III) emission.

$^5D_0$ state lifetime measurements were performed for the Eu-containing samples and the decay curves are shown in Fig. 8. The curves were best-fitted through a monoexponential decay and the calculated $^5D_0$ state lifetime values (τ) are shown in Table 2. The $^5D_0$ state lifetime value of the Eu_2O_3 powder is 0.22 ± 0.01 ms and it decreases to 0.041 ± 0.001 ms after the immobilization probably because the polymer acts as a physical barrier for the UV radiation, decreasing the Eu(III) absorption, and as consequence, decreasing the Eu(III) radiative losses. However, after the cryo-treatment with N_2, the $^5D_0$ state lifetime value increases to 0.081 ± 0.001 ms, showing that the Eu(III) emission is enhancing since the lifetime increase is directly correlated to the enhancement of the radiative losses from the $^5D_0$ state. This observation leads us to conclude that the previously propounded ET mechanism between BO and Eu(III) ions is valid since the emission of the Eu(III) ions is enhancing after the cryo-treatment.

Finally, from the $^5D_0$ state lifetime values and the emission spectra, it is possible to calculate the Eu(III) quantum efficiency (η) by using equations (2)–(5), where A_{rad} and A_{nrad} are the radiative and the non-

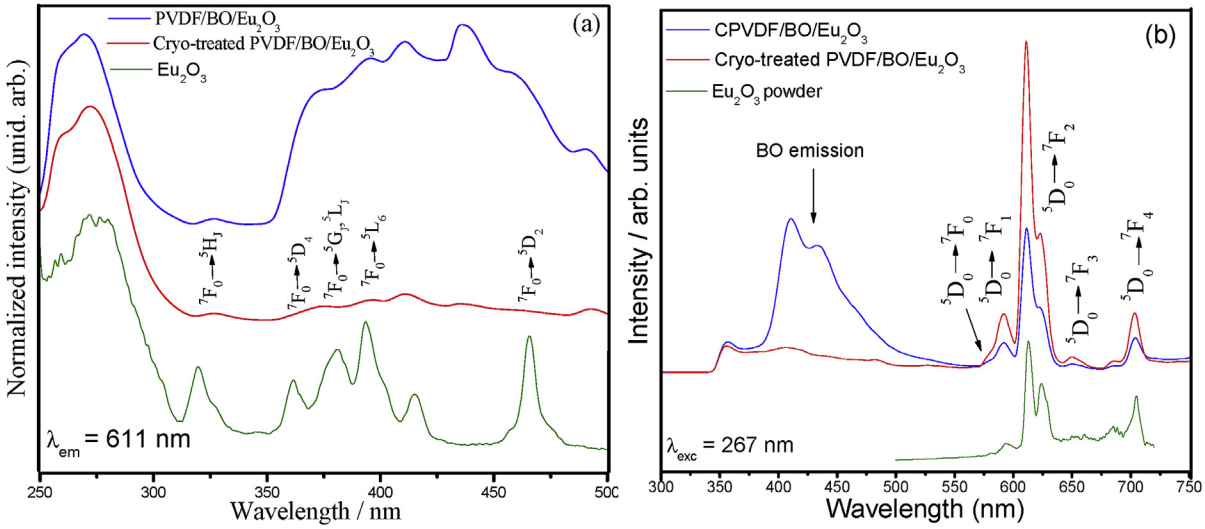

Fig. 7. Excitation (a) and emission (b) spectra of PVDF/BO/Eu_2O_3 membrane before and after the cryo-treatment compared to the Eu_2O_3 powder.

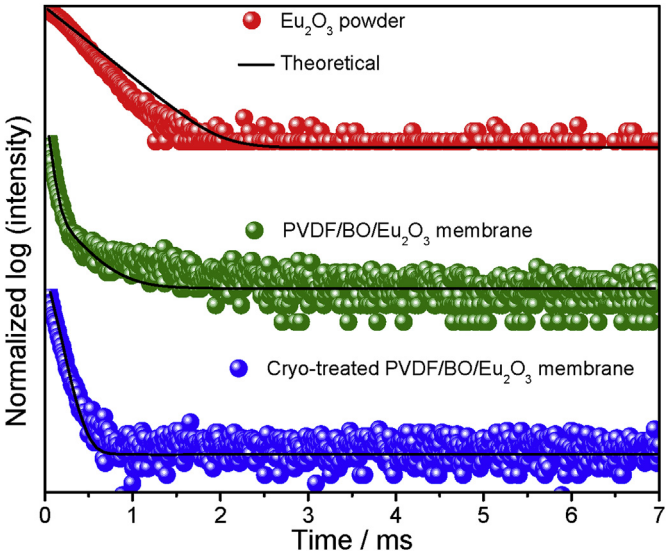

Fig. 8. Experimental decay curves obtained for the PVDF membranes compared to the Eu_2O_3 powder.

Table 2
$^5D_0$ state lifetime (τ) values obtained from a monoexponential fitting in the decay curves shown in Fig. 8, radiative (A_{rad}) e nonradiative (A_{nrad}) rates obtained from the emission spectra and equation (2), and Eu(III)$^5D_0$ level quantum efficiency (η) obtained from equations (2)–(5).

Sample	τ/ms	A_{rad}/s^{-1}	A_{nrad}/s^{-1}	η/%
Eu_2O_3 powder	0.22 ± 0.01	927	3.62 × 103	20
PVDF/BO/Eu_2O_3 membrane	0.041 ± 0.001	383	2.46×10^4	1.0
Cryo-treated PVDF/BO/Eu_2O_3 membrane	0.081 ± 0.001	427	1.21×10^4	4.0

radiative rates for an emitting level, respectively, I is the integrated area under the $^5D_0 \rightarrow {}^7F_j$ transitions in the emission spectra, $\nu_{0\text{-}J}$ is the barycenter energy of the $^5D_0 \rightarrow {}^7F_j$ transition, X is the Lorentz local field correction equal to $n(n^2+2)^2/9$, n is the refractive index equal to 1.426 for the PVDF membranes [54] and 1.590 for the Eu_2O_3 powder [55]; A_{01} can be estimated by the equation $A_{01} = 14.65\ n^3$ in s^{-1} [56].

$$A_{0-\lambda} = A_{0-j} = A_{01}\frac{I_{0-j}}{I_{0-1}}\frac{h\nu_{0-1}}{h\nu_{0-j}} \quad (2)$$

$$\eta = \frac{A_{rad}}{A_{rad} + A_{nrad}} \quad (3)$$

$$A_{rad} = \sum_{J}^{A_{0-j}} \quad (4)$$

$$A_{total} = \frac{1}{\tau} = A_{rad} + A_{nrad} \quad (5)$$

As expected, the Eu(III) quantum efficiency decreases after the polymer immobilization when compared to the Eu_2O_3 powder, as summarized in Table 2. However, the value enhances after the cryo-treatment due to the ET from BO to the Eu(III) ions, as confirmed by the decrease of the BO emission and the increase of the Eu(III) one. In this context, due to this temperature sensitivity, the PVDF/BO/Eu_2O_3 membrane shows potential to be applied in temperature sensor platforms. Despite the Eu(III) quantum efficiency be low, the application of the system is not affected since it depends on just the Eu(III) emission detection that can be easily done by using a simple fluorimeter. Also, as the membrane maintains its properties at room temperature, the system can be exposed to the environment where the temperature will be determined and then, brought back to the room temperature, measuring the photoluminescence. Now, the perspective of the study is quantifying both emissions of the BO and Eu_2O_3 in the membrane as a function of the temperature.

4. Conclusions

The PVDF/BO/Eu_2O_3 composite membranes synthesis by the casting method and the enhanced Eu(III)-red emission played by the cryo-treatment were presented in this study. Insulating micro-structures based on the γ-PVDF phase with bandgap near to 5.90 eV were obtained by drying the membranes at 100 °C, being that Eu_2O_3 particles decrease the PVDF crystallinity. However, after the cryo-treatment, the PVDF crystallinity enhances while its particles became more irregular in shape and more agglomerated. The use of BO also decreases the PVDF thermal stability while the Eu_2O_3 particle addition increases the PVDF stability. The PVDF/Eu_2O_3 composite membrane emits red light under 267 nm excitation characteristic of Eu(III) ions in Eu_2O_3. Furthermore, the Eu(III) red emission under 267 nm excitation enhances after the cryo-treatment, and the unexpected BO emission that occurs by an energy transfer between Eu(III) and BO components is quenched. Finally, even though BO is decreasing PVDF stability, due to the temperature sensitivity between both BO and Eu(III) emissions, the PVDF/Eu_2O_3 membrane shows potential to be applied in low-temperature sensor platforms.

Acknowledgements

The authors are thankful to the Brazilian agencies FAPESP, CNPq and CAPES for the financial research support. Airton G. B. Junior is particularly grateful to the São Paulo research Foundation (FAPESP) for the award of some scholarships (Grant No. 2012/13876-9, 2015/10394-1, and 2016/20421-9). Laboratório de microscopia eletrônica de varredura (FCT/UNESP), laboratório multiusuário de análises químicas (IQ/UNESP) and Laboratório de difração de raios x (FCT/UNESP). LD Carlos from CICECO-Aveiro Institute of Materials (University of Aveiro) is acknowledged for the lifetime measurements.

Appendix A. Supplementary data

Supplementary data to this article can be found online at https://doi.org/10.1016/j.solidstatesciences.2019.04.003.

References

[1] I.V. Taydakov, S.A. Ambrozevich, E.A. Varaksina, A.G. Vitukhnovsky, A.A. Tyutyunov, O.A. Melnik, Luminescent properties of a composite of acrylic polymers doped with Eu(III) complex for ink-jet printing applications, J. Russ. Laser Res. 37 (2016) 192–196.
[2] B. Chen, J. Feng, White-light-emitting polymer composite film based on carbon dots and lanthanide complexes, J. Phys. Chem. C 119 (2015) 7865–7872.
[3] P.A. Raymundo-Pereira, D.A. Ceccato, A.G. Bispo Jr., M.F.S. Teixeira, S.A.M. Lima, A.M. Pires, Study on the structural and electrocatalytic properties of Ba^{2+}- and Eu^{3+}-doped silica xerogels as sensory platforms, RSC Adv. 6 (2016) 104529–104536.
[4] J. Kai, D.F. Parra, H.F. Brito, Polymer matrix sensitizing effect on photoluminescence properties of $Eu3^{+}$-β-diketonate complex doped into poly-β-hydroxybutyrate (PHB) in film form, J. Mater. Chem. 18 (2008) 4549–4554.
[5] S. Lee, J. Park, Luminescent oxygen sensors with highly improved sensitivity based on a porous sensing film with increased oxygen accessibility and photoluminescence, Sens. Actuators, B 249 (2017) 364–377.
[6] R. Aguilar-Sanchez, I. Zelocualtecatl-Montiel, M.J. Galvez-Vazquez, R. Silva-Gonzalez, Analyte-triggered luminescence of Eu^{3+} ions encapsulated in Nafion membranes-preparation of hybrid materials from in membrane chemical reactions, Mater. Chem. Phys. 191 (2017) 206–214.
[7] S. Hameed, P. Predeep, M.R. Baiju, Polymer light emitting diodes - a review on materials and techniques, Rev. Adv. Mater. Sci. 26 (2010) 30–42.
[8] Y. Xu, X. Zhang, J. Peng, Q. Niu, Y. Cao, Efficient polymer white-light-emitting diodes with a phosphorescent dopant, Semicond. Sci. Technol. 21 (2006) 1373–1376.
[9] P. Raju, V. Nandanan, S.K.N. Kuttyl, A study on the use of Castor oil as plasticizer in natural rubber compounds, Prog. Rubber Plast. Recycl. Technol. 23 (2007) 169–180.

[10] Q.X. Chen, P.A. Payne, Industrial applications of piezoelectric polymer transducers, Meas. Sci. Technol. 6 (1995) 249–267.
[11] N. Jia, Q. He, J. Sun, G. Xia, R. Song, Crystallization behavior and electroactive properties of PVDF, P(VDFTrFE) and their blend films, Polym. Test. 57 (2017) 302–306.
[12] Y. Jin, N. Xia, R.A. Gerhardt, Enhanced dielectric properties of polymer matrix composites with $BaTiO_3$ and MWCNT hybrid fillers using simple phase separation, Nanomater. Energy 30 (2016) 407–416.
[13] B.K. Paul, D. Roy, S. Batabyal, A. Bhattacharya, P. Nandy, S. Das, A comparative study of strontium and titanium doped mullite in PVDF matrix and their phase behavior, microstructure and electrical properties, Mater. Chem. Phys. 187 (2016) 119–132.
[14] F. He, K. Lin, D. Shi, H. Wu, H. Huang, J. Chen, F. Chen, K. Lam, Preparation of organosilicate/PVDF composites with enhanced piezoelectricity and pyroelectricity by stretching, Compos. Sci. Technol. 137 (2016) 138–147.
[15] S. Munari, A. Bottino, G. Capannelli, Casting and performance of Polyvinylidene fluoride based membranes, J. Membr. Sci. 16 (1983) 181–193.
[16] N.A. Hashim, Y. Liu, K. Li, Stability of PVDF hollow fibre membranes in sodium hydroxide aqueous solution, Chem. Eng. Sci. 66 (2011) 1565–1575.
[17] M.L.S. Albuquerque, I. Guedes, P. Alcantara, S.G.C. Moreira, N.M.B. Neto, D.S. Correa, S.C. Zílio, J. Braz. Chem. Soc. 16 (2005) 1113.
[18] G.G. Bovi, R.R. Petrus, As C. Pinho, Feasibility of incorporating buriti (Mauritia flexuosa L.) oil nanoemulsions in isotonic sports drink, Int. J. Food Sci. Technol. 52 (2017) 2201–2209.
[19] H.H.F. Koolen, F.M.A. Silva, F.C. Gozzo, A.D.L. Souza, Antioxidant, antimicrobial activities and characterization of phenolic compounds from buriti (Mauritia flexuosa L. f.) by UPLC–ESI-MS/MS, Food Res. Int. 51 (2013) 467–473.
[20] M.L.S. Albuquerque, I. Guedes, P. Alcantara Jr., S.G.C. Moreira, N.M.B. Neto, D.S. Correac, S.C. Zilio, Characterization of buriti (Mauritia flexuosa L.) oil by absorption and emission spectroscopies, J. Braz. Chem. Soc. 16 (2005) 1113–1117.
[21] J.A. Duraes, A.L. Drummond, T.A.P.F. Pimentel, M.M. Murta, S.G.C. Moreira, M.J.A. Sales, Thermal and structural behavior of buriti oil/poly(methyl methacrylate) and buriti oil/polystyrene materials, J. Therm. Anal. Calorim. 92 (2008) 529–534.
[22] D. Schlemmer, E.R. Oliveira, M.J.A. Sales, Polystyrene/thermoplastic starch blends with different plasticizers, J. Therm. Anal. Calorim. 87 (2007) 635.
[23] A.G. Bispo Jr., N.A. Oliveira, C.X. Cardoso, S.A.M. Lima, A.E. Job, I.O. Osorio-Román, C.S. Danna, A.M. Pires, Red-light-emitting polymer composite based on PVDF membranes and europium phosphor using buriti oil as plasticizer, Mater. Chem. Phys. 217 (2018) 160–167.
[24] G. Vicentini, L.B. Zinner, J. Zukerman-Schpector, K. Zinner, Luminescence and structure of europium compounds, Coord. Chem. Rev. 196 (2000) 353–382.
[25] A.G. Bispo Jr., D.A. Ceccato, S.A.M. Lima, A.M. Pires, Red phosphor based on Eu^{3+}-isoelectronically doped Ba_2SiO_4 obtained via sol–gel route for solid state lightning, RSC Adv. 7 (2017) 53752–53762.
[26] H.H. Wang, P. He, H.G. Yan, M.L. Gong, Synthesis, characteristics and lumines-cent properties of a new europium(III) organic complex applied in near UV LED, Sens. Actuators B 156 (2011) 6–11.
[27] A.G. Bispo-Jra, S.A.M. Lima, A.M. Pires, Energy transfer between terbium and europium ions in barium orthosilicate phosphors obtained from sol-gel route, J. Lumin. 199 (2018) 372–378.
[28] S. Kumar, R. Prakash, V.K. Singh, Synthesis, characterization, and applications of europium oxide: a review, Rev. Adv. Sci. Eng. 4 (2015) 247–257.
[29] K.A. Irshad, N.V.C. Shekar, T.R. Ravindran, V. Srihari, K.K. Pandey, X-ray diffraction and Raman studies on Ho: Eu_2O_3, J. Mol. Struct. 1128 (2017) 325–329.
[30] P.M. Martins, P. Martins, V. Correia, J.G. Rocha, S. Lanceros-Mendez, Gd_2O_3:Eu nanoparticle-based poly(vinylidene fluoride) composites for indirect X-ray detection, J. Electron. Mater. 44 (2015) 129–135.
[31] J. Garcia-Torres, P. Bosch-Jimenez, E. Torralba-Calleja, M. Kennedyc, H. Ahmedc, J. Doranc, D. Gutierrez-Tauste, L. Bautista, M.D. Pirriera, Modulating the photo-luminescence of europium-based emitting polymers: influence of the matrix on the photophysical properties, J. Photochem. Photobiol., A 275 (2014) 103–113.
[32] J. Indumathi, J. Bijwe, A.K. Ghosh, M. Fahim, N. Krishnaraj, Wear of cryo-treated engineering polymers and composites, Wear 225–229 (1999) 343–353.
[33] S.K. Karan, A.K. Das, R. Bera, S. Paria, A. Maitra, N.K. Shrivastava, B.B. Khatua, Effect of γ-PVDF on enhanced thermal conductivity and dielectric property of Fe-rGO incorporated PVDF based flexible nanocomposite film for efficient thermal management and energy storage applications, RSC Adv. 6 (2016) 37773–37783.
[34] A. Hartonol, S. Satira, M. Djamal, R. Ramli, H. Bahar, E. Sanjaya, Effect of mechanical treatment temperature on electrical properties and crystallite size of PVDF film, Adv. Mater. Phys. Chem. 3 (2013) 71–76.
[35] R. Gregorio, R.C. Capitao, Morphology and phase transition of high melt temperature crystallized poly(vinylidene fluoride), J. Mater. Sci. 35 (2000) 299–306.
[36] A. Salimi, A.A. Yousefi, Conformational changes and phase transformation mechanisms in PVDF solution-cast films, J. Polym. Sci., Part B: Polym. Phys. 42 (2004) 3487–3495.
[37] J. Hirschinger, D. Schaefer, H.W. Spiess, A.J. Lovinger, Chain dynamics in the crystalline γ-phase of poly(vinylidene fluoride) by two-dimensional exchange deuteron NMR, Macromolecules 24 (1991) 2428–2433.
[38] J. Song, C. Lu, D. Xu, Y. Ni, Y. Liu, Z. Xu, J. Liu, The effect of lanthanum oxide (La_2O_3) on the structure and crystallization of poly(vinylidene fluoride), Polym. Int. 59 (2010) 954–960.
[39] F. Shi, J. Ma, P. Wang, Y. Ma, Effect of quenching temperatures on the morphological and crystalline properties of PVDF and PVDF–TiO2 hybrid membranes, J. Taiwan Inst. Chem. Eng. 43 (2012) 980–988.
[40] J. Indumathi, J. Bijwe, A.K. Ghosh, M. Fahim, N. Krishnaraj, Wear of cryo-treated engineering polymers and composites, Wear 225–229 (1999) 343–353.
[41] M.M. Pavlick, W.S. Johnson, B. Jensen, E. Weiser, Evaluation of mechanical properties of advanced polymers for composite cryotank applications, Compos Part A Appl Sci 40 (2009) 359–367.
[42] J.S.C. Campos, A.A. Ribeiro, C.X. Cardoso, Preparation and characterization of PVDF/$CaCO_3$ composites, J. Mater. Sci. Eng. B 136 (2007) 123–128.
[43] L.F. Malmonge, L.H.C. Mattoso, Thermal analysis of conductive blends of PVDF and poly(o-methoxyaniline), Polymer 41 (2000) 8387–8391.
[44] F.S. Al-Hazmi, D.M. de Leeuw, A.A. Al-Ghamdi, F.S. Shokr, Synthesis and characterization of novel Cu_2O/PVDF nanocomposites for flexible ferroelectric organic electronic memory devices, Curr. Appl. Phys. 17 (2017) 1181–1188.
[45] W.E. Mahmoud, A.M.Y. El-Lawindy, M.H. El Eraki, H.H. Hassan, Butadiene acrylonitrile rubber loaded fast extrusion furnace black as a compressive strain and pressure sensors, Sens. Actuators A Phys. 136 (1) (2007) 229–233.
[46] V. Sencadas, S. Lanceros-Méndez, J.F. Mano, Characterization of poled and non-poled-PVDF films using thermal analysis techniques, Thermochim. Acta 424 (2004) 201–207.
[47] A.K. Srivastava, H.S. Virk, 50 MeV lithium ion beam irradiation effects in poly vinylidene fluoride (PVDF) polymer, Bull. Mater. Sci. 23 (2000) 533–538.
[48] A. Pal Indolia, M.S. Gaur, Optical properties of solution grown PVDF-ZnO nanocomposite thin films, J. Polym. Res. 20 (2013) 1–8.
[49] H.M. Alhusiki-Alghamdi, N.S. Alghunaim, Spectroscopic studies of nanocomposites based on PEO/PVDF blend loaded by SWCNTs, J. Mod. Phys. 6 (2015) 414–424.
[50] A.B. Murphy, Band-gap determination from diffuse reflectance measurements of semiconductor films, and application to photoelectrochemical water-splitting, Solar Sol. Energy Mater. Sol. Cells 91 (2007) 1326–1337.
[51] P. Kubelka, F. Munk, Ein Beitrag zur Optik der Farbanstriche, Z. Tech. Phys. 15 (1931) 593–601.
[52] B. Ahmed, S.K. Raghuvanshi, N.P. Siddhartha, J.B.M. Sharma, M.A. WAHAB, 1.25 MeV gamma irradiated induced physical and chemical changes in poly vinylidene fluoride (PVDF), Polymer. Apr. 2 (2013) 42–46.
[53] W.T. Carnall, G.L. Goodman, K. Rajnak, R.S. Rana, A systematic analysis of the spectra of the lanthanides doped into single crystal LaF_3, J. Chem. Phys. 90 (1989) 3443–3457.
[54] C. Duan, W. Mei, W. Yin, J. Liu, J.R. Hardy, M. Bai, S. Ducharme, Theoretical study on the optical properties of polyvinylidene fluoride crystal, J. Phys. Condens. Matter 15 (2003) 3805–3811.
[55] G.H.A. Melo, J.D.M. Dias, T.A. Lodi, M.J. Barboza, F. Pedrochi, A. Steimacher, Optical and spectroscopic properties of Eu_2O_3 doped CaBAl glasses, Opt. Mater. 54 (2016) 98–103.
[56] A.G. Bispo Jr., G.M.M. Shinohara, Ana M. Pires, Celso X. Cardoso, Red phosphor based on Eu3+-doped Y2(MoO4)3 incorporated with Au NPs synthesized via Pechini's method, Opt. Mater. 84 (2018) 137–145.